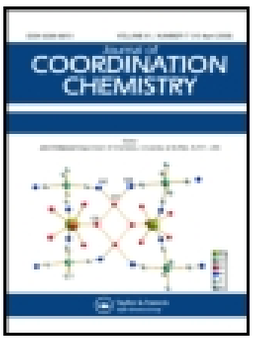

Journal of Coordination Chemistry

ISSN: 0095-8972 (Print) 1029-0389 (Online) Journal homepage: http://www.tandfonline.com/loi/gcoo20

Crystal structure and cytotoxic activities of a bis(pyrrolyl-imine) gold(III) complex

Daniel De Moraes Profirio, Raphael Enoque Ferraz De Paiva, Camilla Abbehausen, Alexandre Cuin, Norberto Masciocchi, Daisy Machado, Marcelo Lancellotti, Pedro Paulo Corbi & André Luiz Barboza Formiga

To cite this article: Daniel De Moraes Profirio, Raphael Enoque Ferraz De Paiva, Camilla Abbehausen, Alexandre Cuin, Norberto Masciocchi, Daisy Machado, Marcelo Lancellotti, Pedro Paulo Corbi & André Luiz Barboza Formiga (2016): Crystal structure and cytotoxic activities of a bis(pyrrolyl-imine) gold(III) complex, Journal of Coordination Chemistry, DOI: 10.1080/00958972.2016.1214949

To link to this article: http://dx.doi.org/10.1080/00958972.2016.1214949

Publisher: Taylor & Francis
Journal: *Journal of Coordination Chemistry*
DOI: http://dx.doi.org/10.1080/00958972.2016.1214949

Crystal structure and cytotoxic activities of a bis(pyrrolyl-imine) gold(III) complex

DANIEL DE MORAES PROFIRIO†, RAPHAEL ENOQUE FERRAZ DE PAIVA†, CAMILLA ABBEHAUSEN†, ALEXANDRE CUIN‡, NORBERTO MASCIOCCHI§, DAISY MACHADO¶, MARCELO LANCELLOTTI¶, PEDRO PAULO CORBI† and ANDRÉ LUIZ BARBOZA FORMIGA*†

†Institute of Chemistry, University of Campinas, PO Box 6154, Campinas, SP, Brazil, 13083-970
‡Federal University of Juiz de Fora, Juiz de Fora, MG, Brazil, 36036-330
§Dipartimento di Scienza e Alta Tecnologia, Universita degli Studi dell'Insubria, 22100, Como, Italy
¶ Institute of Biology, University of Campinas, PO Box 6109, Campinas, SP, Brazil, 13471-083

A gold(III) complex with N,N'-ethylenebis(pyrrol-2-yl-methyleneamine) (H_2pyren) was synthesized and characterized by physicochemical and spectroscopic measurements. Density functional theory (DFT) studies and cytotoxic assays were performed. Infrared, mass spectrometry and ^{1}H, ^{13}C and $\{^{15}N,^{1}H\}$ nuclear magnetic resonance analyses indicate that pyren is deprotonated and gold(III) is four coordinate in a square planar environment, with the pyrrole and imine nitrogens as donors. The structure was confirmed by powder X-ray diffraction and confirmed as a minimum of the potential energy surface by DFT. Cytotoxic activity of $[Au(pyren)]^{+}$ was active against three tumorigenic cell lines with IC_{50} values of 35 μM. Interaction studies with CT-DNA by fluorescence and competition with ethidium bromide (EB) showed a quenching of the emission band of DNA with a Stern-Volmer quenching constant value of $(3.0 \pm 0.1)\times10^{4}$ M^{-1} and a decrease in fluorescence quenching of EB-DNA system, respectively, confirming that DNA is a possible target for the complex via an intercalative binding, which was confirmed by DNA conformational changes observed with circular dichroism spectroscopy.

Keywords: Pyrrolyl-imine; Gold(III); DFT; Cytotoxic activity; DNA

*Corresponding author. Email: formiga@iqm.unicamp.br

1. Introduction

Gold(III) complexes have been studied for their antitumor activity since the 1980s, and several compounds were reported to be more effective than the clinically used metallodrug cisplatin [1-3]. However, most of them were reduced in biological medium to gold(I) or colloidal gold [1, 4]. A few examples were reported to exhibit significant antitumor activity and solution stability [5]. Reduction of gold(III) to gold(I) and covalent binding of gold ions to biomolecular targets have been proposed to account for the cytotoxicity of gold(III) compounds. For example, peptide and protein containing methionine residues as well as disulfide bonds can reduce gold(III) to gold(I) [6, 7].

Porphyrin ligands stabilize gold(III) complexes and are studied for their biological applications [8]. Historically, gold(III) compounds were proposed to act as cisplatin (DNA covalent binding) due to the isoelectronic and isostructural characteristics of gold(III) and platinum(II) [1, 4, 9, 10]. However, demetallation and release of gold(III) for metalloporphyrin complexes are very unlikely. DNA intercalation is another possible mechanism for gold-porphyrin complexes due to their rigid planar structure [11].

Thioredoxin and proteasome have also been proposed as targets considering that $[Au(porphyrin)]^+$ compounds are planar lipophilic cations. The use of planar lipophilic cations to target mitochondria in cancer cells has been explored as a possible strategy [12-14]. Sun and co-workers [15] studied a series of Au(III)-porphyrin complexes in order to understand the structure/activity relationship. For all the synthesized complexes the reported activities vary from non-toxic to compounds with a very low IC_{50} concentration when accessed against nasopharyngeal tumorigenic cell lines. The observations are attributed to the lipophilicity of the complexes, in agreement with the previous reported bisphosphine gold(I) complexes [16,17].

Schiff base ligands and their complexes have been studied to elucidate various aspects of catalytic activity, magnetic, spectroscopic and anticancer properties, as well as the role of metal ions in biological systems. Although salicylidimine ligands and their complexes have been extensively studied in this context, only few data are known about the Schiff base ligands derived from pyrrole-2-carboxaldehyde and aliphatic or aromatic diamines, bis(pyrrol-2-yl-methyleneamine) or bis(pyrrolyl-imine) [18]. Coordination of these ligands to metal ions usually occurs with deprotonation of the pyrrole NH groups, yielding tetradentate and dianionic ligands [19].

Examples of complexes with this class of ligands include chelates of Ru(II) [20], Pd(II) [21], Ni(II) [21-25], Cu(II) [24, 26-28], Mn(II) [29], Zn(II) [30-35] and Pt(II) [36, 37]. Recently, the synthesis and biological reactivity of stable nitroxyl-bound {FeNO} species [38, 39] were also reported.

However, there is little information about Au(III) complexes with pyrrolyl-imine ligands. Recently a patent about bis(pyrrolyl-imine) and bis(imidazolyl-imine) Schiff base gold(III) complexes as chemotherapeutic agents [40] and the biodistribution of a ^{198}Au-labelled gold(III) chelate with a bis(pyrrolyl-imine) Schiff base ligand [41] were reported. The present work describes the synthesis, spectroscopic characterization and cytotoxic assays of a cationic gold(III) complex with the tetradentate Schiff base ligand N,N'-ethylenebis(pyrrol-2-yl-methyleneamine) ($C_{12}H_{14}N_4$, H_2pyren), which is represented in figure 1. For the complex $[Au(pyren)]^+$, 'pyren' corresponds to the dianionic form of H_2pyren $(pyren)^{2-}$.

2. Experimental

2.1. *Materials*

All reagents used in this study were of analytical grade and used without purification, except for ethylenediamine which was distilled before use. Ethylenediamine, pyrrole-2-carboxaldehyde, $H[AuCl_4]$ and a solution of tetrabutylammonium hydroxide ($[Bu_4N]OH$) in water (1.0 M) were purchased from Sigma-Aldrich Laboratories. Acetonitrile, ethanol and dichloromethane were purchased from Synth. Deoxyribonucleic acid sodium salt from calf thymus (CT-DNA) was purchased from Sigma-Aldrich Laboratories and a solution (expressed as nucleotides) was prepared in 10 mM $NaClO_4$ and dialyzed for 24 h.

2.2. *Synthesis of H_2pyren*

H_2pyren was prepared using a method described in the literature [26]. Pyrrole-2-carboxaldehyde (1.11 g, 11.7 mmol) and ethylenediamine (500 µL, 7.5 mmol) were dissolved in 10 mL of ethanol. The mixture was stirred for a while and then 10 drops of glacial acetic acid were added. After a few seconds a white precipitate formed. The suspension was stirred at room temperature for 2 h. The white solid was collected by filtration, washed with cold ethanol and dried under vacuum. The compound was purified by recrystallization from ethanol with a total yield of 1.70 g (68%). Anal. Calc. for H_2pyren, $C_{12}H_{14}N_4$ (MW = 214.12): C, 67.2; H, 6.53; N, 26.1 %. Found:

C, 67.3; H, 6.09; N, 26.2 %. ESI-MS m/z 215.2 $[H_2pyren + H]^+$. This ligand is soluble in methanol, DMSO, dimethylformamide, chloroform, acetone and is insoluble in diethyl ether and n-hexane.

2.3. *Synthesis of [Au(pyren)](PF$_6$)*

The gold(III) complex with H_2pyren was synthesized according to a similar procedure reported by Munro and co-workers [40]. First, a solution (1.0 M) of $[Bu_4N]OH$ (3.6 mL, 3.6 mmol) was added to a solution of $H[AuCl_4]$ (0.99 g, 3.0 mmol) in distilled water (15 mL). The mixture was stirred at room temperature for 1 h and the yellow solid obtained corresponding to $[Bu_4N][AuCl_4]$ was collected by filtration, washed with distilled water and dried in vacuum (80% yield). Further, NH_4PF_6 (0.24 g, 1.49 mmol) was dissolved in 10 mL of ethanol and the resulting solution was added to a stirring suspension of H_2pyren (0.23 g, 1.12 mmol) in 8 mL of dichloromethane. To this suspension, a solution of $[Bu_4N][AuCl_4]$ (0.14 g, 0.37 mmol) in 10 mL of dichloromethane was added dropwise. The reaction mixture was heated under reflux for 1 h and then cooled to room temperature. The orange-brown reaction mixture was capped and put in the freezer (-20 °C) overnight to induce precipitation of an orange solid. The product was collected by filtration, washed with dichloromethane and dried in vacuum. The sample was purified by washing with water (4 × 5 mL), followed by filtration and drying in vacuum. 150 mg of an orange solid was obtained (74% yield). Anal. Calc. for [Au(pyren)](PF_6), $C_{12}H_{12}N_4PF_6Au$ (MW = 554.2): C, 26.0; H, 2.16; N, 10.1 %. Found: C, 25.6; H, 1.64; N, 10.1 %. ESI-MS m/z 409.1 $[Au(pyren)]^+$. The complex is soluble in acetonitrile, DMSO, dimethylformamide, acetone and insoluble in chloroform, diethyl ether and n-hexane. No single crystals were obtained even after several attempts by slow evaporation and solvent diffusion. The complex is stable in solution for several hours and only after mixing with a sodium citrate dihydrate solution (200 µL, 500 µM), $[Au(pyren)]^+$ (10 mL, 100 µM, acetonitrile) showed some evidence of decomposition or reduction of gold(III), as observed in figure S1.

2.4. *Physical measurements*

Elemental analyses for carbon, hydrogen and nitrogen were performed using a CHNS/O Perkin Elmer 2400 Analyzer. Infrared (IR) spectra from 4000 to 400 cm^{-1} were measured using an ABB Bomen MB Series Model B100 with resolution of 4 cm^{-1}; samples were prepared as KBr pellets.

Solution-state ^{1}H, ^{13}C and the {^{15}N,^{1}H} HMBC nuclear magnetic resonance spectra were recorded for H_2pyren and $[Au(pyren)]^+$ on a Bruker Avance III 400 MHz (9.395T). Samples were analyzed in deuterated acetonitrile-d_3 solutions and the chemical shifts were given relative to tetramethylsilane (TMS). The UV-Vis spectra were recorded in acetonitrile solutions (30 µM for H_2pyren, 100 µM for [Au(pyren)](PF_6)) from 200-1100 nm using 10.00 mm quartz cuvettes in a Hewlett-Packard 8453A diode array spectrophotometer. Electrospray ionization mass spectrometry (ESI-MS) measurements were carried out in a Waters Synapt HDMS instrument (Manchester, UK). The ligand and the complex were dissolved in H_2O/MeCN 50:50 with 0.1% (v/v) formic acid at a concentration of 1.0 mg cm^{-3} and further diluted 100-fold in the same solvent. The resulting solutions were directly infused into the instrument ESI source at a flow rate of 15 µL min^{-1}. Typical acquisition conditions were capillary voltage of 3 kV sampling cone voltage of 20 V, source temperature of 100 °C, desolvation temperature of 200 °C, cone gas flow of 30 L h^{-1} and desolvation gas flow of 900 L h^{-1}. Thermogravimetric and differential thermal analysis (TGA/DTA) were performed on a simultaneous TGA/DTA Seiko Exstar 6000 Thermoanalyzer using the following conditions: synthetic air, flow rate of 50 cm^3 min^{-1} and heating rate of 10 °C min^{-1}, from 25 °C to 1000 °C.

2.5. *Structural analysis by X-ray powder diffraction data*

The polycrystalline [Au(pyren)](PF_6) powder was gently ground in an agate mortar and then deposited in the hollow of Silicon zero-background plate sample-holder. The diffraction data were collected by overnight scans (in recycling mode) in the 2θ range of 4-105° with steps of 0.02° using a Bruker AXS D8 Advanced diffractometer, equipped with Ni-filtered Cu-Kα radiation (λ=1.5418 Å), a Lynxeye linear position-sensitive detector PSD and the following optics: primary beam Soller slits (2.3°), fixed divergence slit (0.3°), receiving slit (8 mm). The generator was set at 40 kV and 40 mA. Standard peak search, followed by indexing through the single-value decomposition approach [42] implemented in TOPAS [43], allowed detection of the approximate unit cell parameters. Since *a* axis (20.17 Å) is nearly double than *b* axis (10.04 Å) many Bragg peaks of the 0*kl* were overlapped with *h*0*l*, making the space group assignment troublesome. In the present case, LeBail refinement in the space group *Pban* and *Pcan* afforded very similar R_{wp}'s, and careful inspection of systematic absences did not solve the space group ambiguity. Structure solutions, performed by the simulated annealing (SA) technique [44]

implemented in TOPAS, were attempted in both space groups, eventually leading to a chemically plausible model only when *Pcan* was chosen. In the structure solution process, a rigid body model for half organic ligand, idealized as Z matrix formalism, flexible at few torsion angles (figure 1) was used where the twofold axis passes through the imaginary center of the aliphatic -CH_2-CH_2- vector, placed at the special position x, 0.5, 0.25. In the same way, PF_6^- ions were also assembled as half PF_6^- (idealized as geometrical Cartesian coordinates) where the phosphorus is lying on a twofold axis at special position x, 0.00, 0.75. The single Au(III) was found to lie on a special position x, 0.50, 0.25. In the final refinement, carried out by the Rietveld method [45], the rigid bodies used in the SA step were maintained and the angles between C_4-C_5=N, C_6-N-C_5 and C_3-C_4-C_5 were also refined, leading to a total of 54 optimized parameters, including background coefficients (of the Chebyshev's type) and spherical harmonics coefficients for anisotropic peak broadening. Also, a single P-F bond distance and an isotropic thermal parameter for gold (B_{Au}; lighter atoms were given a common isotropic thermal parameter, set at $B_{iso} = B_{Au} + 2.0$ Å^2) were refined in the final steps. The final Rietveld refinement plot for [Au(pyren)](PF_6) is given as Supplementary Material (figure S2).

2.6. *Fluorescence studies*

The fluorescence emission spectra of a 100 μM CT-DNA solution in $NaClO_4$ 10 mM were recorded from 300-500 nm before and after addition of a $[Au(pyren)]^+$ solution in acetonitrile (final concentrations = 20, 30, 40, 50, 60 and 70 μM) using an excitation wavelength of 260 nm in a Varian Cary Eclipse fluorescence spectrophotometer. For the EB-DNA binding experiment a solution of CT-DNA (100 μM) was prepared in buffer solutions containing 10 mM $NaClO_4$. Stock solutions of CT-DNA incubated with ligand at a r_i of 0.2 and complex at a r_i of 0.1, 0.2 (r_i being the ratio compound/nucleotide), both in DMSO, were prepared and incubated at 37 °C for 24 h. Increasing amounts of EB in the range 0-0.05 of ethidium bromide per nucleotide were added to CT-DNA and CT-DNA treated with H_2pyren and $[Au(pyren)]^+$. The experiments were performed in triplicate, setting the excitation at 525 nm and monitoring the emission at 600 nm in a Varian Cary Eclipse fluorescence spectrophotometer. During the period of UV-Vis and fluorescence analyses (approx. 6 h) the complex remained stable and did not show evidence of decomposition in solution.

2.7. *Circular dichroism*

Circular dichroism spectra of a 100 μM CT-DNA solution in $NaClO_4$ 10 mM were recorded after addition of a $[Au(pyren)]^+$ solution in DMSO at various ratios (r_i = 0.0-0.50, where r_i is the ratio of compound per nucleotide) and incubation at 37 °C for 24 h. The CD spectra were obtained at room temperature on a Jasco J720 ORD 306 spectropolarimeter using 10.00 mm quartz cuvettes with a 450 W xenon lamp. Eight scans were recorded for a 225-320 nm spectral window at a 20 nm min^{-1} rate. The complex also remained stable in solution during the acquisition period of circular dichroism spectra (approx. 5 h).

2.8. *Molecular modeling*

Geometric optimizations were carried out using GAMESS software [46] with a convergence criterion of 10^{-4} a.u. in a conjugate gradient algorithm. The LANL2TZ [47] effective core potential and basis set (including relativistic effects) were used for gold and the atomic 6-31G(d,p) basis set [48-51] for all other atoms. Density functional theory (DFT) calculations were performed by using the PBE0 [52] gradient-corrected hybrid functional to solve the Kohn-Sham equations with a 10^{-5} a.u. convergence criterion for the density change and the final geometries were confirmed as minima of the potential energy surface (PES).

The harmonic vibrational frequencies and intensities were calculated at the same level of theory with the analytical evaluation of second derivatives of energy as a function of atomic coordinates. Frequencies were scaled by a factor of 0.9547, as recommended by Merrick, Moran and Radom [53]. To simulate electronic spectra, time dependent DFT calculations were performed in the same level of theory to calculate the 20-first singlet excited states of both molecules.

2.9. *Cytotoxic assays*

Lung adenocarcinomic alveolar basal epithelial cells (A549), prostate cancer cells (PC3), endometrial adenocarcinoma cells (HEC1B) and mouse embryonic fibroblast cells (Balb/ 3T3) were cultured in Dulbecco's modified eagle's medium (DMEM) supplemented with 10% of fetal calf serum (FCS), using streptomycin and penicillin as antibiotics, in an atmosphere of 5% CO_2 at 37 °C. All cell culture reagents were purchased from Costar (Corning Inc., NY). The 3-(4,5-dimethylthiazol-2-yl)-2,5-diphenyltetrazolium salt (MTT) was acquired from Sigma. Cells were

placed in a 96-well plate (5×10^3 cells/well) 24 h prior to the beginning of the experiment. Stock solutions of H_2pyren and $[Au(pyren)]^+$ were prepared in DMSO in a concentration of 10 mM. The compounds were diluted into the cells medium in order to achieve different concentrations (100 - 3.125 μM). Forty-eight hours after addition of the complex, MTT salt was added (aiming for a final concentration of 0.50 mg mL^{-1}) and the cells were incubated with this reagent for a period of 3 h [54]. After the incubation period, cells were washed with PBS and isopropanol was added. The cell viability was determined by absorbance measurements at 570 nm.

3. Results and discussion

3.1. *Structure of $[Au(pyren)]^+$*

Mass spectrometry suggests the existence of the $[Au(pyren)]^+$ in solution (figure S4) and the solid state composition with one equivalent of PF_6^- as a counter ion is suggested by elemental and thermal analyses (figure S5). The crystal structure of $[Au(pyren)](PF_6)$ was obtained using state-of-the-art powder diffraction data measured on conventional laboratory X-ray diffractometer equipment. Even if some limitations are present, due to extensive use of molecular modeling by partially flexible rigid bodies an imposed special positions for Au(III) ions, pyren and PF_6^- counter ions, some fruitful comments on the intramolecular features are here provided. Fortunately, significant information such as stoichiometry, molecular conformation and connectivity and overall crystal packing features are well-defined by combining X-ray powder diffraction results with DFT studies and spectroscopic and analytical evidences. A summary of crystal data of $[Au(pyren)](PF_6)$ and data collection parameters is presented in table 1. The molecular structure of the $[Au(pyren)](PF_6)$ complex, drawn using SCHAKAL [55], is depicted in figure 2.

Au(III) ions lie on the plane of the four nitrogens of pyren that form a distorted square planar coordination environment. Due to the geometry of the ligand, the bite angle N_{im}-Au-N'_{im} determined as 78.14° by X-ray powder diffraction, is lower than the ideal for a square planar geometry. Even if the ligand adopts a planar configuration for the nitrogens, the ethylene bridge is distorted and the torsion angle N_{im}-C6-C6'-N'_{im} obtained in the solid state structure is 19.08°. Selected experimental distances and angles can be found in table 2.

In order to get insight into the spectra of samples, DFT calculations were performed for H_2pyren and its Au(III) complex using the hybrid PBE0 and a basis set of triple-zeta quality. A

comparison between the DFT equilibrium geometry obtained for the $[Au(pyren)]^+$ complex (figure 3b) and diffraction data reveal that the square planar configuration is well reproduced with Au(III) lying in the plane of the four nitrogens. Experimental Au(III)-N distances are very well-reproduced by calculations (table 2) and values are in the range found for $[Au(salen)]^+$ and analogues, with bond distances around 2.00 Å [56]. Some bond angles are different when experimental and theoretical values are compared but this can be explained by the fact that packing effects are not taken into account in the theoretical model.

The geometry obtained for the free ligand (figure 3a) is in good agreement with crystallographic data for a similar bis(pyrrolyl-imine) ligand [19]. The geometry around each imine group corresponds exclusively to the *E*-isomer, consistent with the fact that the *Z*-isomer would lead to unfavorable steric interactions between the pyrrole NH groups and adjacent methylene groups of the ethyl bridge. Moreover, the structure exhibits an all-staggered conformation for the CH_2 groups of the ethyl chain and an *anti*-configuration for the two pyrrolyl-imine units. Comparison between the optimized geometries of complex and free ligand reveals that coordination changes some bond distances by 0.02 Å. As expected, these geometrical changes are related with the differences of free and coordinated H_2pyren IR spectra as will be discussed in the following section.

3.2. *Infrared vibrational spectroscopy*

IR spectra of H_2pyren and $[Au(pyren)]^+$ are shown in figure S6. The IR spectrum of H_2pyren exhibits the (N-H) stretch of the pyrrole group at 3178 cm^{-1}. The asymmetric and symmetric (C-H) stretches of CH_2 can be observed at 2941 and 2871 cm^{-1}, respectively. A sharp and intense signal at 1641 cm^{-1} corresponds to the characteristic (C=N) stretch of imino-group. Moreover, the (C_{Ar}-N) stretch of the pyrrole ring at 1288 cm^{-1} and the (C-H) out-of-plane deformation of heteroaromatic compounds at 829 cm^{-1} are also observed [28].

The $[Au(pyren)]^+$ IR spectrum supplies evidence of coordination of the ligand to Au(III). The first evidence is the absence of the (N-H) stretch, due to loss of the hydrogen of the pyrrole group upon coordination. Furthermore, the (C=N) stretch of imino group is shifted 64 cm^{-1} to lower wavenumbers. The spectra suggest participation of both the pyrrole and imino groups in coordination of H_2pyren to Au(III). The presence of two new bands can be assigned to PF_6^-, the (P-F) stretching ν_3 at 840 cm^{-1} and the (F-P-F) deformation ν_4 at 559 cm^{-1} [57].

The simulated IR spectra of H_2pyren and $[Au(pyren)]^+$ are in agreement with the experimental spectra, confirming all the assignments made in table 3. The simulated (N-H) stretching mode in the H_2pyren spectrum appears at 3545 and 3534 cm^{-1}. Experimental absorptions in the IR spectrum of H_2pyren at 2941, 2871 and 1641 cm^{-1} were confirmed by simulated spectra as the (C-H) asymmetric, symmetric and (C=N) stretching modes, respectively. The simulated spectrum also shows that the (C=N) stretching mode was shifted to lower energy by 83 cm^{-1} and the absence of the (N-H) stretching mode, which corroborates to the proposition of tetradentate coordination.

3.3. *Nuclear magnetic resonance spectroscopy*

Solution state ^1H, ^{13}C and [^1H-^{15}N] heteronuclear multiple bond coherence (HMBC) NMR spectra were obtained in order to confirm the coordination mode of H_2pyren to Au(III). The spectra of $[Au(pyren)]^+$ were analyzed by comparison to the NMR spectra of the free ligand. The structure of H_2pyren with numbering for assignments is shown in figure 1.

The obtained ^1H-NMR spectrum for H_2pyren is presented in figure S7. For the ligand, hydrogens of the ethylene bridge appear as a singlet at 3.74 ppm. The hydrogens of the pyrrole ring appear in the region of aromatic protons as triplet (H2, 6.10 ppm with ^3J = 3.2 Hz), doublet of doublets (H3, 6.43 ppm with ^3J = 3.4 Hz and ^4J = 1.2 Hz) and multiplet (H1, 6.86 ppm). The hydrogens of imino-group (C=N) also appear as a singlet at 8.08 ppm, [31] and this deshielding can be ascribed to the anisotropy of the C=N bond [58].

The obtained ^1H-NMR spectrum for $[Au(pyren)]^+$ is presented in figure S8. The hydrogens of the ethylene bridge appear as a singlet at 4.41 ppm. The hydrogens of the pyrrole ring appear in the region of aromatic protons as doublet of doublets (H2, 6.48 ppm with ^3J = 4.2 and 2.1 Hz), doublet (H3, 7.07 ppm with ^3J = 4.3 Hz) and doublet (H1, 7.45 ppm with ^3J = 1.4 Hz). The hydrogens of imino group (C=N) also appear as a singlet at 7.85 ppm.

Table 4 contains the assignments of hydrogens, chemical shifts and $\Delta\delta$ ($\delta_{complex} - \delta_{ligand}$) values for H_2pyren and $[Au(pyren)]^+$. Observing the $\Delta\delta$ values in table 4, all proton resonances of H_2pyren are shifted downfield upon coordination, consistent with donation of electronic density to Au(III). However, the hydrogens of imino are shifted upfield.

The obtained ^{13}C-NMR spectra for H_2pyren and $[Au(pyren)]^+$ are presented in figure S9, and table 4 summarizes the carbon chemical shifts and assignments [31] for H_2pyren and the

[Au(pyren)]$^+$ complex. For the ligand, carbons of the ethylene bridge (C6) appear at 61.4 ppm, as expected for alkane groups substituted by heteroatoms. The carbons of pyrrole appear in the region of heteroaromatic compounds at 109.3 (C2), 113.6 (C3), 121.8 (C1) and 130.6 (C4) ppm, while the carbons of imino group (C5) appear at 152.6 ppm due to the effect of hybridization (C sp^2) and electronegativity of the nitrogen [59]. Table 4 shows that changes for the carbons follow the same pattern as observed for the hydrogens upon coordination, with all carbons shifted downfield, consistent with donation of electronic density of pyren to Au(III).

Nitrogen coordination of the pyrrole and imino groups of H_2pyren to Au(III) was evaluated by {^{15}N,^{1}H} multiple bond coherence NMR spectroscopy. The ^{15}N spectrum of H_2pyren is provided in figure S10. In the H_2pyren spectrum, the ^{15}N chemical shift of the nitrogens of the pyrrole and imino groups are observed at 146 ppm and 303 ppm, as expected [59], respectively. In the [Au(pyren)]$^+$ spectrum these signals shift to 186 ppm (N of pyrrole) and 208 ppm (N of imino group), as observed in figure S10.

For nitrogens of pyrrole a deshielding was observed and can be assigned as a σ-donation of a pair of electrons by the deprotonated ligand to Au(III). However, changes in the anisotropy upon coordination could cause shielding of nitrogens of imino group. The signals observed of 40 ppm for pyrrole and -95 ppm for the imino as well as the symmetry retained in the ^{1}H, ^{13}C and {^{15}N,^{1}H} spectra confirm a tetradentate coordination mode of H_2pyren to Au(III).

3.4. *Electronic absorption spectroscopy*

The experimental UV-Vis spectrum of H_2pyren (figure 4a) shows an intense absorption at 284 nm (ε = 55000 $M^{-1}cm^{-1}$). The presence of shoulders clearly indicates that this band is composed by more than one transition, as confirmed by TD-DFT calculations. At least three transitions give the band at 250-300 nm and all of them can be assigned as pyrrole π-π* transitions with a small contribution from the imine nitrogens. All calculated transitions and the corresponding orbitals are provided as Supplementary Material (table S1 and figure S11).

The large number of transitions in the experimental UV-Vis spectrum of [Au(pyren)]$^+$ is well reproduced by theory (figure 4b). The nature of the transitions in the 250-500 nm range can be assigned as pyrrole π-π* transitions as inspection of table S2 and figure S12 reveal. An intense ligand-to-metal charge transfer (LMCT) is predicted at 212 nm by TD-DFT. This transition would originate from a σ-bonding orbital between pyren and the Au(III) $5d_{xy}$ orbital

(orbital #61, figure S12) and the LUMO orbital which is mainly the Au(III) $5d_{x^2-y^2}$ orbital (#66, figure S12).

3.5. *Cytotoxic studies*

Based on the fact that Au(III) compounds with tetradentate dianionic ligands would behave similarly to lipophilic organic cations, which have been suggested as potential anti-cancer drug candidates [60], we proposed that the $[Au(pyren)]^+$ complex can act as a lipophilic cation. In order to preliminarily explore the cytotoxic behavior of $[Au(pyren)]^+$, the complex was assayed for its cytotoxic activities in comparison to the free ligand.

The evaluation was performed *in vitro* using concentrations varying from 3.125 μM to 100 μM for lung adenocarcinomic alveolar basal epithelial cells (A549), prostate cancer cells (PC3), endometrial adenocarcinoma cells (HEC1B) and for mouse embryonic fibroblast cells (Balb/3T3), as shown in figure S13. The results show that H_2pyren has no significant cytotoxic effect in the concentrations tested for all cells excluding HEC1B, which seems to be the most sensitive among the tested ones. For HEC1B it was possible to find an IC_{50} concentration for H_2pyren of 54.6±0.3 μM. Even for HEC1B the IC_{50} of the $[Au(pyren)]^+$ is much lower than the free ligand being 28.0±0.2 μM. For the other cell lines the $[Au(pyren)]^+$ complex showed activity with IC_{50} values of 37.2±0.3, 39.0±0.2 and 35.8±0.2 μM for Balb/3T3, A549 and PC3, respectively. So, considering that H_2pyren has no significant activity it is possible to suggest that the rigid and cationic structure of $[Au(pyren)]^+$ is fundamental for cytotoxic activity. Nevertheless, the complex did not show selective cytotoxic activity over the tumoral and non-tumoral cells. For HEC1B, the IC_{50} value is slightly lower than that of Balb/3T3.

In comparison with other Au(III) complexes with N-donor ligands, the complex $[Au(pyren)]^+$ displayed higher cytotoxicity than $[Au(bipy)Cl_2]^+$ (bipy = 2,2´-bipyridine), $[Au(en)Cl_2]^+$ (en = ethylenediamine), $[Au(dach)Cl_2]^+$ (dach = 1,2-diaminocyclohexane) and cisplatin in lung adenocarcinomic cells, as observed in table 5. For the other tumorigenic cell lines the $[Au(pyren)]^+$ complex showed a lower cytotoxicity, even when compared to cisplatin. Furthermore $[Au(TPP)]^+$, where TPP = tetraphenylporphyrin, displayed promising anticancer activities toward a panel of human cancer cell lines including nasopharyngeal carcinoma (SUNE1, CNE1, CNE2 and C666-1), promyelocytic leukemia (HL-60), hepatocellular carcinoma (HepG2), cervical epithelioid carcinoma (HeLa) and oral epidermoid carcinoma (KB-

3-1 and KB-V1) with IC_{50} values between 0.11 and 0.73 μM [8, 61]. DNA intercalation and the use of planar lipophilic cations to target mitochondria in cancer cells have been proposed as a possible mechanism for $[Au(porphyrin)]^+$ compounds due to their planar and cationic structure [11, 12].

3.6. *DNA Binding studies*

Cytotoxic studies showed the activity of $[Au(pyren)]^+$ against tumorigenic cell lines. So, interaction studies with DNA, a possible biological target, were performed since $[Au(pyren)]^+$ is a planar and cationic compound that can interact with DNA by intercalation, a common interaction mode between small molecules and DNA [68].

A structural feature of all intercalators is that they possess an extended, electron-deficient and planar aromatic ring systems. When a ligand intercalates into the DNA stack, the bases must be separated by approximately 3.4 Å to accommodate the ligand [69]. The consequences of DNA intercalation by exogenous molecules have attracted considerable interest in medicinal chemistry, because such a complex formation leads to significant modification of the DNA structure and may result in a suppressed function of the nucleic acid in physiological processes, leading to cell death [70].

In this context fluorescence spectral analysis was performed to investigate the binding properties of the $[Au(pyren)]^+$ to DNA. The emission spectra of CT-DNA in the absence and presence of a $[Au(pyren)]^+$ solution in acetonitrile with increasing concentrations are shown in figure 5, where the emission band at 340 nm is attributed to CT-DNA when it is excited at 260 nm. The complex $[Au(pyren)]^+$ is non-fluorescent under the experimental conditions.

Fluorescence quenching has been widely studied both as a fundamental phenomenon and as a source of information about biochemical systems. These biochemical applications of quenching are due to the molecular interactions that result in quenching. Both static and dynamic quenching require molecular contact between the fluorophore and quencher [71].

The fluorescence spectra (figure 5) showed a quenching of the emission band of CT-DNA with increasing concentrations of $[Au(pyren)]^+$. According to DFT and spectroscopic studies the complex shows a square planar coordination environment which allows the $[Au(pyren)]^+$ complex to intercalate with DNA. Furthermore, the overall charge on the cationic

complex favors electrostatic interactions with the negatively charged phosphate backbone of the DNA double helix [40].

Both static and dynamic quenching of fluorescence can be described by the Stern-Volmer equation:

$$\frac{Io}{I} = 1 + Ksv[Q] \qquad (1)$$

where I_0 and I are the fluorescence intensities in the absence and presence of quencher, respectively, K_{SV} is the Stern-Volmer quenching constant and [Q] is the concentration of quencher. A plot of I_0/I versus [Q] yields an intercept of one on the *y*-axis and a slope equal to K_{SV}. The graphic obtained for the $[Au(pyren)]^+$-DNA system is shown in figure S14. The Stern-Volmer plot illustrates that the quenching of DNA by the complex is in agreement (Pearson's r = 0.994) with equation 1. The K_{SV} value for $[Au(pyren)]^+$ was $(3.0 \pm 0.1)\times10^4$ M^{-1}, which is a low value in comparison with the heterocyclic cationic dye "nile blue" ($K_{SV} = 3.2\times10^6$ M^{-1}) [72] and Pt(II) complexes containing 2,2'-bipyridine and 1,10-phenanthroline ligands ($K_{SV} \approx 10^5$ M^{-1}) [73].

Static suppression is observed if fluorophore and suppressor interact by stacking-based interactions. This is the basic interaction mode between nucleotides and planar aromatic suppressors. $[Au(pyren)]^+$-DNA interactions are proposed to be static and, in this case, K_{SV} also represents the formation constant for the complex $[Au(pyren)]^+$-DNA [71].

The ability of $[Au(pyren)]^+$ to bind to CT-DNA was also investigated by competition experiments with EB because it is a well-known intercalative probe. In the competitive binding experiments, the EB-DNA system showed the characteristic strong emission at 600 nm when excited at 525 nm, indicating that the intercalated EB molecules were sufficiently protected from quenching by polar solvent molecules by the neighboring base pairs of DNA [68]. Upon increasing the concentration of $[Au(pyren)]^+$, a decrease in emission of the EB-DNA system was observed, as seen in figure 6. These results support a competitive binding mode for $[Au(pyren)]^+$ with EB, indicating that the DNA is a possible target for the complex with an intercalative binding mode.

Conformational changes on CT-DNA upon addition of $[Au(pyren)]^+$ were analyzed by circular dichroism spectroscopy (CD) to confirm these differences. Spectral studies of DNA

employed ultraviolet light within the range 180-300 nm, where the pair bases of DNA absorb [74].

Interactions between the $[Au(pyren)]^+$ complex and CT-DNA are shown in figure 7. B-form oligonucleotides are characterized by a positive long wavelength band at 260-280 nm and a negative band around 245 nm. However, the position and amplitude of the CD bands show marked differences in terms of sequence diversity [75]. In the circular dichroism spectra (figure 7), a concentration-dependent alteration is observed where the structure is clearly ordered but distinct from free DNA. This slight alteration may be due to an intercalative binding mode since significant changes in the DNA structure are not observed for this interaction mode. The complex showed a slight red-shift and an increase in the negative signal at 240-250 nm as well as the presence of a isodichroic point at 255 nm, which suggests the presence of equilibrium conformations [76, 77]. Similar changes of the CD spectra of DNA have been previously observed upon interaction of cisplatin [78] and $[AuCl_2(esal)]$ with DNA [79].

To conclude, the results obtained in this work by fluorescence spectroscopy, competition with ethidium bromide and circular dichroism spectroscopy showed that DNA is a possible biological target of $[Au(pyren)]^+$, which corroborates with the results previously reported by Munro and coworkers [40].

4. Conclusion

A gold(III) complex with a bis(pyrrolyl-imine) ligand (H_2pyren) was synthesized and characterized by different spectroscopic techniques, as well as theoretical calculations using DFT. The complex showed significant, but not selective, cytotoxic activity against three tumorigenic cell lines and one non-tumorigenic fibroblast cell line with IC_{50} values in the μM range, comparable with cisplatin and other gold(III) complexes with N-donor ligands.

The obtained results show that the rigid and cationic $[Au(pyren)]^+$ structure is important for cytotoxic activity and a mechanism of action was investigated with fluorescence studies, competition assays with ethidium bromide and circular dichroism spectroscopy. The results revealed that DNA is a possible biological target for the complex with an interaction mode by intercalation, leading to a small modification of the DNA structure.

Supplementary material

Crystal data, fractional atomic coordinates and displacement parameters of [Au(pyren)](PF_6) crystal structure are supplied in standard CIFs deposited in the Cambridge Crystallographic Data Centre (1045938). The data can be obtained free of charge at http://www.ccdc.cam.ac.uk/conts/retrieving.html [or from the Cambridge Crystallographic Data Centre (CCDC), 12 Union Road, Cambridge CB2 1EZ, UK; Fax: +44 (0) 1223-336033; E-mail: deposit@ccdc.cam.ac.uk]. Several spectra are provided as supplementary materials such as ^{1}H and ^{13}C NMR, mass spectra, and IR spectra. The thermal decomposition profile of the complex is also available. Files with cartesian coordinates for DFT optimized geometries of H_2pyren and $[Au(pyren)]^+$ are also available for download.

Acknowledgements

This study was supported by grants from FAPESP (Fundação de Amparo à Pesquisa do Estado de São Paulo, proc. no. 2012/08230-2) and CNPq (Conselho Nacional de Desenvolvimento Científico e Tecnológico, proc. no. 130697/2012-5, 402627/2012-1 and 442123/2014-0). Computational facilities at the National High-Performance Computing Center in Sao Paulo (CENAPAD-SP) are gratefully acknowledged.

References

[1] C.F. Shaw. *Chem. Rev.*, **99**, 2589 (1999).

[2] P. Bruijnincx, P.J. Sadler. *Curr. Opin. Chem. Biol.*, **12**, 197 (2008).

[3] A. Cuin, A.C. Massabni, G.A. Pereira, C.Q.F. Leite, F.R. Pavan, R. Sesti-Costa, T.A. Heinrich, C.M. Costa-Neto. *Biomed. Pharmacother.*, **65**, 334 (2011).

[4] E.R.T. Tiekink. *Crit. Rev. Oncol. Hematol.*, **42**, 225 (2002).

[5] L. Messori, G. Marcon, M.A. Cinellu, M. Coronnello, E. Mini, C. Gabbiani, P. Orioli. *Bioorg. Med. Chem.*, **12**, 6039 (2004).

[6] E.A. Pacheco, E.R. Tiekink, M.W. Whitehouse, *Gold Chemistry: Applications and Future Directions in the Life Sciences*, Wiley VCH Verlag, Weinheim (2009).

[7] B.D. Glišić, U. Rychlewska, M.I. Djuran. *Dalton Trans.*, **41**, 6887 (2012).

[8] Y. Wang, Q.Y. He, R.W.-Y. Sun, C.M. Che, J.F. Chiu. *Cancer Res.*, **65**, 11553 (2005).

[9] S.J. Berners-Price, A. Filipovska. *Metallomics*, **3**, 863 (2011).

[10] I. Ott. *Coord. Chem. Rev.*, **253**, 1670 (2009).

[11] S. Nobili, E. Mini, I. Landini, C. Gabbiani, A. Casini, L. Messori. *Med. Res. Rev.*, 550 (2009).

[12] P.J. Barnard, S.J. Berners-Price. *Coord. Chem. Rev.*, **251**, 1889 (2007).

[13] A. Bindoli, M.P. Rigobello, G. Scutari, C. Gabbiani, A. Casini, L. Messori. *Coord. Chem. Rev.*, **253**, 1692 (2009).

[14] V. Milacic, Q.P. Dou. *Coord. Chem. Rev.*, **253**, 1649 (2009).

[15] R.W.-Y. Sun, C.K.L. Li, D.-L. Ma, J.J. Yan, C.-N. Lok, C.H. Leung, N. Zhu, C.-M. Che. *Chem.-Eur. J.*, **16**, 3097 (2010).

[16] P.J. Barnard, M.V. Baker, S.J. Berners-Price, D.A. Day. *J. Inorg. Biochem.*, **98**, 1642 (2004).

[17] M.J. McKeage, S.J. Berners-Price, P. Galettis, R.J. Bowen, W. Brouwer, L. Ding, L. Zhuang, B.C. Baguley. *Cancer Chemother. Pharmacol.*, **46**, 343 (2000).

[18] A.A. Khandar, C. Cardin, S.A. Hosseini-Yazdi, J. McGrady, M. Abedi, S.A. Zarei, Y. Gan. *Inorg. Chim. Acta*, **363**, 4080 (2010).

[19] O.Q. Munro, G.L. Camp. *Acta Crystallogr. Sect. C: Cryst. Struct. Commun.*, **C59**, o672 (2003).

[20] C. Stern, F. Franceschi, E. Solari, C. Floriani, N. Re, R. Scopelliti. *J. Organomet. Chem.*, **593**, 86 (2000).

[21] A. Bacchi, M. Carcelli, L. Gabba, S. Ianelli, P. Pelagatti, G. Pelizzi, D. Rogolino. *Inorg. Chim. Acta*, **342**, 229 (2003).

[22] C.J. Jones, J. McClever. *J. Chem. Soc. A*, **8**, 1052 (1971).

[23] X.F. Shan, L.Z. Wu, X.Y. Liu, L.P. Zhang, C.H. Tung. *Eur. J. Inorg. Chem.*, **21**, 3315 (2007).

[24] J.M. Chen, W.J. Ruan, L. Meng, F. Gao, Z.A. Zhu. *Spectrochim. Acta, Part A*, **71A**, 191 (2008).

[25] J.P. Holland, P.J. Barnard, S.R. Bayly, J.R. Dilworth, J.C. Green. *Inorg. Chim. Acta*, **362**, 402 (2009).

[26] L.Y. Yang, Q.Q. Chen, Y. Li, S.X. Xiong, G.P. Li, J.S. Ma. *Eur. J. Inorg. Chem.*, **7**, 1478 (2004).

[27] Y. Wang, W.N. Wu, Q. Wang, Z.Y. Yang. *J. Coord. Chem.*, **63**, 147 (2010).

[28] W. Li, Y. Wang, L. Yang, A. Szeghalmi, Y. Ye, J. Ma, M. Luo, J. Hu, W. Kiefer. *J. Raman Spectrosc.*, **38**, 483 (2007).

[29] F. Franceschi, G. Guillemot, E. Solari, C. Floriani, N. Re, H. Birkedal, P. Pattison. *Chem. Eur. J.*, **7**, 1468 (2001).

[30] Z.K. Wu, Q.Q. Chen, S.X. Xiong, B. Xin, Z.W. Zhao, L.J. Jiang, J.S. Ma. *Angew. Chem. Int. Ed. Engl.*, **42**, 3271 (2003).

[31] L.Y. Yang, Q.Q. Chen, G.Q. Yang, J.S. Ma. *Tetrahedron*, **59**, 10037 (2003).

[32] L.C. Liang, P.Y. Lee, W.L. Lan, C.H. Hung. *J. Organomet. Chem.*, **689**, 947 (2004).

[33] Q.H. Yuan, L.J. Wan. *Chem. Eur. J.*, **12**, 2808 (2006).

[34] Y. Wang, Z.Y. Yang, Z.N. Chen. *Bioorg. Med. Chem. Lett.*, **18**, 298 (2008).

[35] Y. Wang, Z. Wu, Z. Cao, L. Kang, H. Fu, J.S. Ma, J. Yao, B.H. Loo. *Colloids Surf. A*, **329**, 44 (2008).

[36] H.F. Xiang, S.C. Chan, K.K.Y. Wu, C.M. Che, P.T. Lai. *Chem. Commun.*, **11**, 1408 (2005).

[37] X.F. Shan, D.H. Wang, C.H. Tung, L.Z. Wu. *Tetrahedron*, **64**, 5577 (2008).

[38] A.K. Patra, K.S. Dube, B.C. Sanders, G.C. Papaefthymiou, J. Conradie, A. Ghosh, T.C. Harrop. *Chem. Sci.*, **3**, 364 (2012).

[39] B.C. Sanders, A.K. Patra, T.C. Harrop. *J. Inorg. Biochem.*, **118**, 115 (2013).

[40] O.Q. Munro, K.J. Akerman, P. Akerman, *Gold Complexes for Use in the Treatment of Cancer*. Patent Number WO2011158176 (2012).

[41] M.P. Akerman, O.Q. Munro, M. Mongane, J.A. van Staden, W.I.D. Rae, C.J. Bester, B.M. Painter, Z. Szucs, J.R. Zeevaart. *J. Labelled Comp. Radio-pharm.*, **56**, 530 (2013).

[42] A. Coelho. *J. Appl. Cryst.*, **36**, 86 (2003).

[43] TOPAS-R Software, version 3.0, Bruker AXS, Karlsruhe, Germany (2005).

[44] A. Coelho. *J. Appl. Cryst.*, **22**, 899 (2000).

[45] R.A. Young, *The Rietveld Method*, Oxford University Press, New York (1981).

[46] M.W. Schmidt, K.K. Baldridge, J.A. Boatz, S.T. Elbert, M.S. Gordon, J.H. Jensen, S.K.N. Matsunaga, K. Nguyen, S. Su, T.L. Windus, M. Dupuis, J.A.J. Montgomery. *J. Comput. Chem.*, **14**, 1347 (1993).

[47] L.E. Roy, P.J. Hay, R.L. Martin. *J. Chem. Theory Comput.*, **4**, 1029 (2008).

[48] R. Ditchfie, W.J. Hehre, J.A. Pople. *J. Chem. Phys.*, **54**, 724 (1971).

[49] W.J. Hehre, R. Ditchfie, J.A. Pople. *J. Chem. Phys*., **56**, 2257 (1972).

[50] P.C. Harihara, J.A. Pople. *Theor. Chim. Acta*, **28**, 213 (1973).

[51] M. M. Francl, W. J. Pietro, W. J. Hehre, J. S. Binkley, M. S. Gordon, D. J. DeFrees, J. A. Pople. *J. Chem. Phys*., **77**, 3654 (1982).

[52] C. Adamo, V. Barone. *J. Chem. Phys*., **110**, 6158 (1999).

[53] J. P. Merrick, D. Moran, L. Radom. *J. Phys. Chem. A*, **81**, 11683 (2007).

[54] T. Mosmann. *J. Immunol. Methods*, **65**, 55 (1983).

[55] E. Keller. *Chem. Unserer Zeit*., **20**, 178 (1986).

[56] R. W. Y. Sun, C. M. Che. *Coord. Chem. Rev*., **253**, 1682 (2009).

[57] K. Nakamoto. *Infrared and Raman Spectra of Inorganic and Coordination Compounds Part A*, 6th Edn, Wiley Publication, New York (2009).

[58] T. J. Batterham. *NMR spectra of simple heterocycles*, Wiley Interscience Publication, United States (1973).

[59] R. M. Silverstein, F. X. Webster, D. J. Kiemle. *Spectrometric identification of organic compounds*, 7th Edn, Wiley Interscience Publication, United States (2005).

[60] V. R. Fantin, M. J. Berardi, L. Scorrano, S. J. Korsmeyer, P. Leder. *Cancer Cell*, **2**, 29 (2002).

[61] Y. F. To, R. W. Y. Sun, Y. Chen, V. S. F. Chan, W. Y. Yu, P. K. H. Tam, C. M. Che, C. L. S. Lin. *Int. J. Cancer*, **124**, 1971 (2009).

[62] M. Arsenijevic, M. Milovanovic, V. Volarevic, A. Djekovic, T. Kanjevac, N. Arsenijevic, S. Dukic, Z. D. Bugarcic. *Med. Chem.*, **8**, 2 (2012).

[63] M. M. U. Mehboob, M. Altaf, M. Fettouhi, A. A. Isab, M. I. Wazeer, M. N. Shaikh, S. Altuwaijri. *Polyhedron*, **61**, 225 (2013).

[64] S. S. A. Jaroudi, M. Fettouhi, M. I. M. Wazeer, A. A. Isab, S. Altuwaijri. *Polyhedron*, **50**, 434 (2013).

[65] P. Zhang, W. Y. Gao1, S. Turner, B. S. Ducatman. *Mol. Cancer*, **2**, 1 (2003).

[66] S. Dhara, F. X. Gub, R. Langerb, O. C. Farokhzad, S. J. Lippard. *Proc. Natl. Acad. Sci. U.S.A*., **105**, 17356 (2008).

[67] H. N. Nguyen, B. U. Sevin, H. Averette, J. Perras, R. Hightower, R. Ramos, D. Donato, M. Penalver. *Cancer Chemother. Pharmacol*., **30**, 37 (1992).

[68] Z. F. Chen, Y. C. Liu, Y. Peng, X. Hong, H. H. Wang, M. M. Zhang, H. Liang. *J. Biol. Inorg. Chem.*, **17**, 247 (2012).

[69] G. M. Blackburn, M. J. Gait, D. Loakes, D. M. Williams. *Nucleic Acids in Chemistry and Biology*, 3rd Edn, RSC Publishing (2006).

[70] H. Ihmels, K. Faulhaber, D. Vedaldi, F. DallAcqua, G. Viola, *Photochem. Photobiol.*, **81**, 1107 (2005).

[71] J. R. Lakowicz, *Principles of Fluorescence Spectroscopy*, 3rd Edn, Springer (2006).

[72] Q. Y. Chen, D. H. Li, Y. Zhaob, H. H. Yang, Q. Z. Zhua, J. G. Xu. *Analyst*, **124**, 901 (1999).

[73] N. Shahabadi, S. Mohammadi, R. Alizadeh. *Bioinorg. Chem. Appl.*, **124**, 1 (2011).

[74] J. Kypr, I. Kejnovska, D. Renciuk, M. Vorlickova. *Nucleic Acids Res.*, **37**, 1713 (2009).

[75] Y.-M. Chang, C. K. M. Chen, M.-H. Hou. *Int. J. Mol. Sci.*, **13**, 3394 (2012).

[76] D. W. Gruenwedel, M. K. Cruikshank, G. M. Smith. *J. Inorg. Biochem.*, **52**, 251 (1993).

[77] M. E. Holtzer, A. Holtzer. *Biopolymers*, **32**, 1675 (1992).

[78] M. Gay, A. M. Montana, V. Moreno, M. J. Prieto, R. Llorens, L. Ferrer. *J. Inorg. Biochem.*, **99**, 2387 (2005).

[79] P. Calamai, A. Guerri, L. Messori, P. Orioli, G. P. Speroni. *Inorg. Chim. Acta*, **285**, 309 (1999).

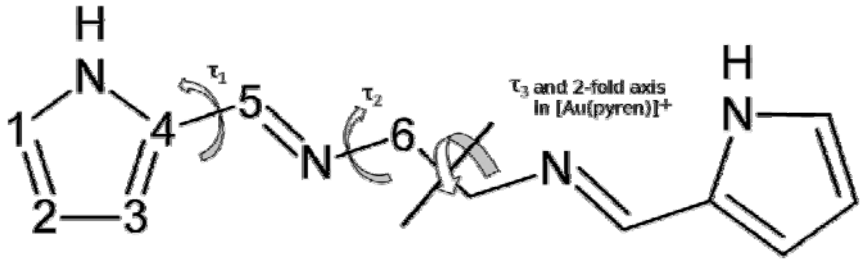

Figure 1. Schematic structure of N,N'-ethylenebis(pyrrol-2-yl-methyleneamine) (H_2pyren) with carbon numbering. Hydrogens are omitted for clarity. The torsion angles refined in the powder diffraction analysis are indicated as τ_1, τ_2 and τ_3.

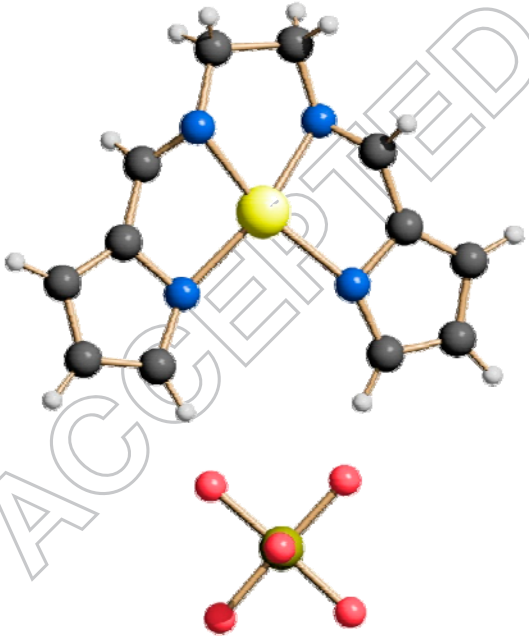

Figure 2. SCHAKAL plot of [Au(pyren)](PF_6) complex. Au(III) ion is yellow, carbon, hydrogen and nitrogen atoms are dark gray, white and blue, respectively, and symmetry code x, 1-y, 0.5-z was used to generate complete pyren ligand. Fluorine and phosphorus are presented in red and

dark yellow, respectively, and the whole counter-ion PF_6^- was generated applying x, -y, 1.5-z symmetry code.

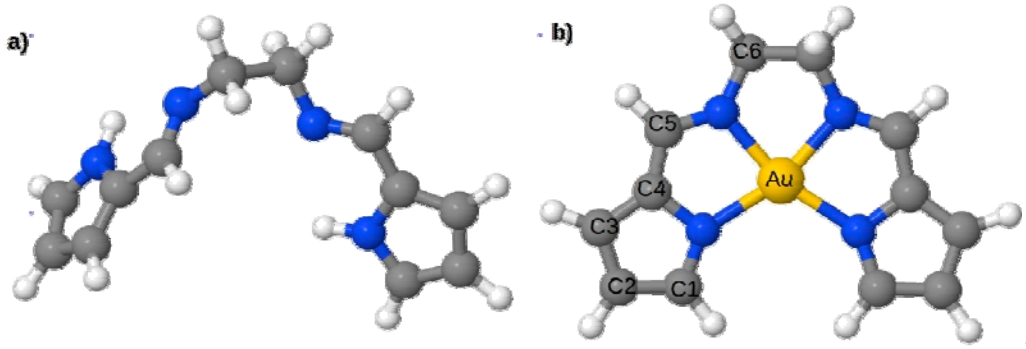

Figure 3. Optimized structure for a) H_2pyren and b) $[Au(pyren)]^+$ obtained by DFT using PBE0/LANL2TZ/6-31G(d,p).

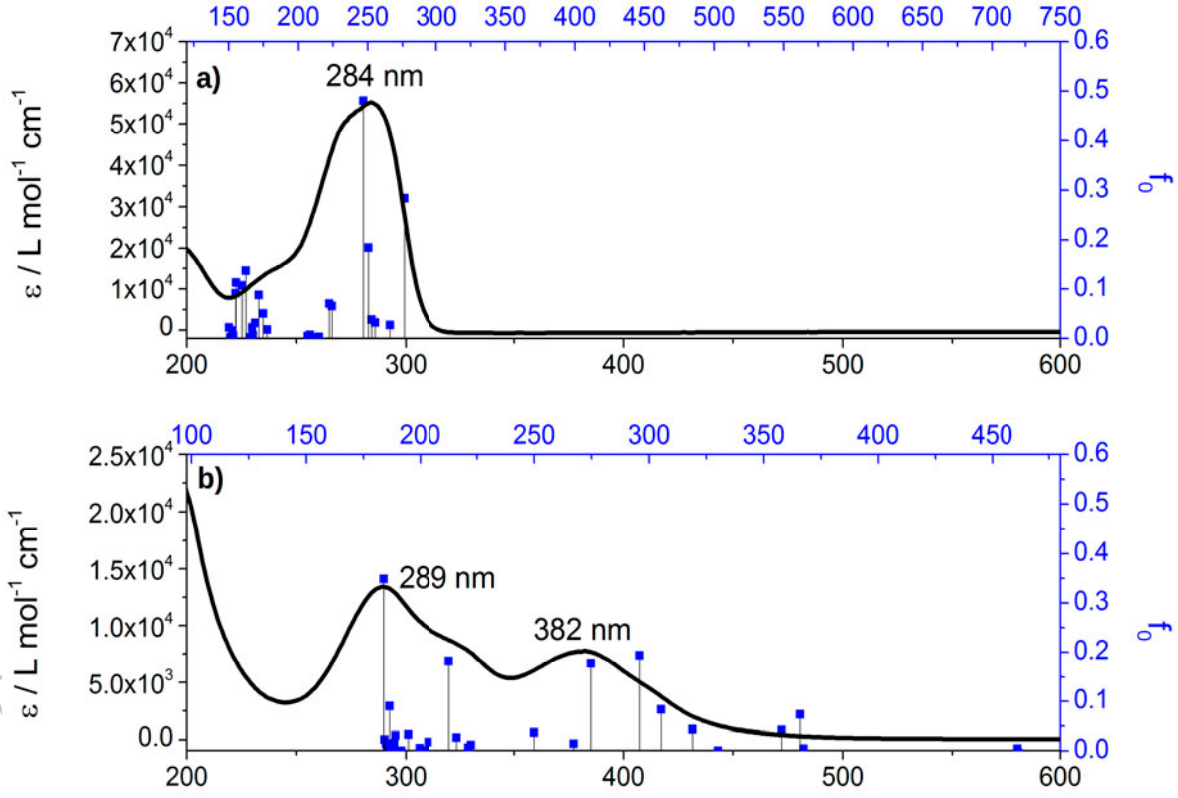

Figure 4. Experimental UV-Vis spectra obtained in acetonitrile (solid lines) and theoretical transitions (vertical lines) of a) H_2pyren and b) $[Au(pyren)]^+$. TD-DFT calculations were performed in the PBE0/LANL2TZ/6-31G(d,p) level of theory.

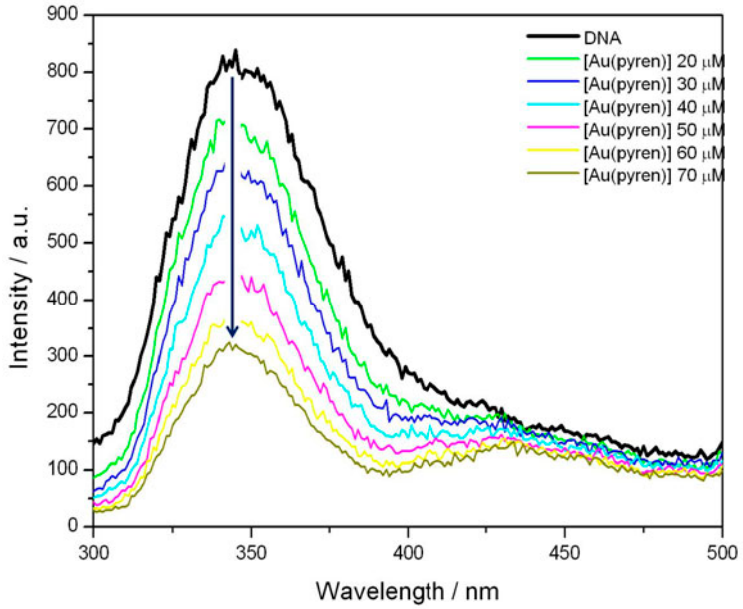

Figure 5. Fluorescence spectra of CT-DNA solutions in the absence and presence of $[Au(pyren)]^+$ in increasing concentrations. The arrow indicates the spectral change upon complex titration.

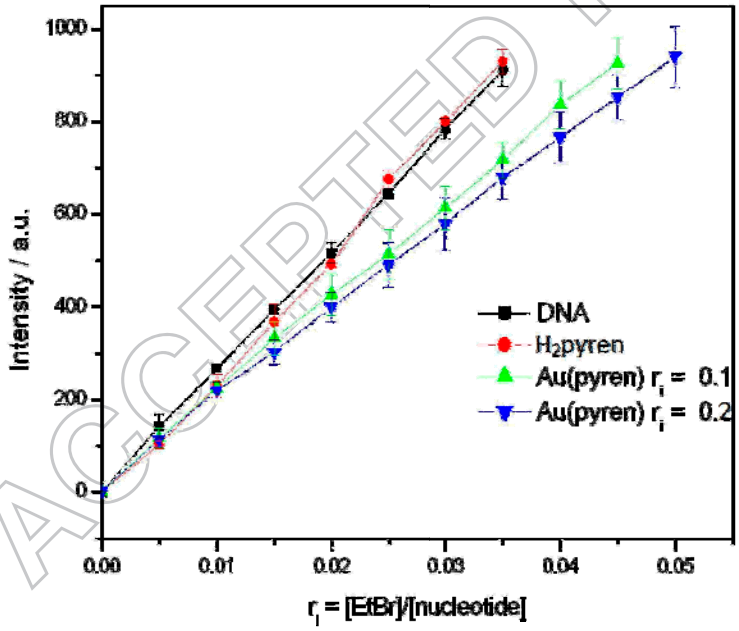

Figure 6. Ethidium bromide/DNA emission with λ_{em} = 600 nm after incubation with H_2pyren and $[Au(pyren)]^+$ for 24 h.

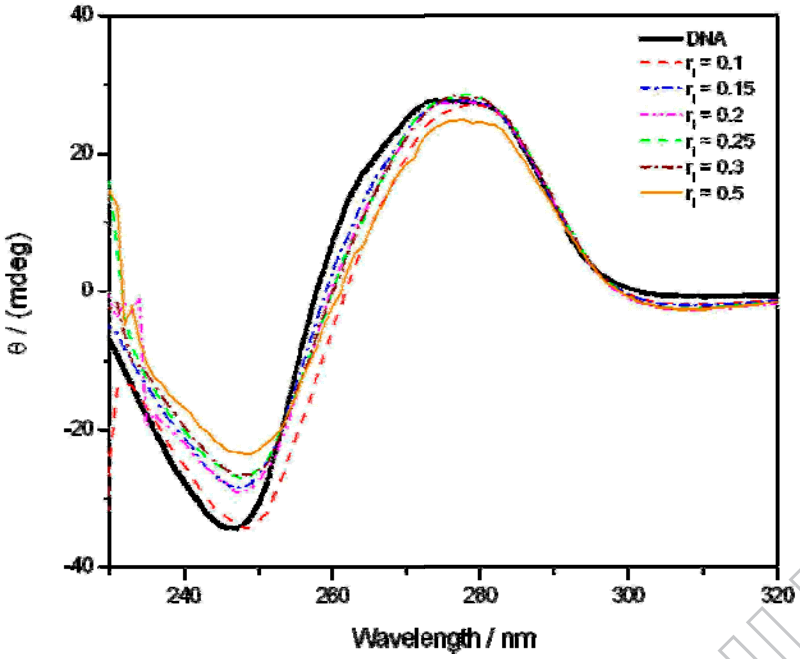

Figure 7. Circular dichroism spectra of CT-DNA alone and CT-DNA incubated with $[Au(pyren)]^+$ at different r_i values.

Table 1. Crystallographic data of [Au(pyren)](PF_6).

Empirical formula	$C_{12}H_{12}AuF_6N_4P$
Formula weight (g mol^{-1})	554.18
T (K)	298
λ(CuKα) (Å)	1.5418
Crystal system	Orthorhombic
Space group	*Pcan*
a (Å)	20.1732(4)
b (Å)	10.0373(2)
c (Å)	8.2463(2)
V ($Å^3$)	1669.75(7)
Z	4
d_{calc} (g cm^{-3})	2.204
μ (mm^{-1})	18.2
F(000)	1040
Number of parameters	54
R_{Bragg}, R_{wp}	0.053 / 0.077

Table 2. Selected experimental (PXRD) and theoretical (PBE0/LANL2TZ/6-31G(d,p)) geometrical parameters obtained for H_2pyren and $[Au(pyren)]^+$.

	Theoretical		Experimental[a]
	H_2pyren	$[Au(pyren)]^+$	$[Au(pyren)]^+$
Distances / Å			
C1-N_{pyr}	1.357	1.335	1.390[b]
C1-C2	1.383	1.404	1.390[b]
C2-C3	1.412	1.387	1.390[b]
C3-C4	1.387	1.406	1.390[b]
C4-N_{pyr}	1.368	1.397	1.390[b]
C4-C5	1.442	1.397	1.450
C5-N_{im}	1.277	1.314	1.280
C6-N_{im}	1.440	1.464	1.460
C6-C6'	1.531	1.534	1.540
Au-N_{im}	---	1.985	1.987
Au-N_{pyr}	---	2.023	2.033
Angles / °			
C1-N_{pyr}-C4	110.1	107.9	108.0
C5-N_{im}-C6	118.0	130.6	120.8
N_{pyr}-Au-N_{im}	---	81.2	95.29
N_{pyr}-Au-N'$_{pyr}$	---	114.0	96.12
N_{im}-Au-N'$_{im}$	---	83.3	78.14
N_{pyr}-Au-N'$_{im}$	---	164.5	161.0
Dihedral angles / °			
N_{im}-C6-C6'-N'$_{im}$	66.3	39.4	19.1
N_{pyr}-C4-C5-N_{im}	0.2	2.3	60.5
C4-C5-N_{im}-C6	180.0	167.9	180.0

[a] Symmetry code: x, 1 - y, 0.5 - z; [b] Fixed value in the Z-matrix formalism

Table 3. Theoretical values obtained by DFT (PBE0/LANL2TZ/6-31G(d,p)) for H_2pyren and $[Au(pyren)]^+$ from 4000 and 400 cm^{-1}.

Assignment	Theoretical / cm^{-1}		Experimental / cm^{-1}	
	H_2pyren	$[Au(pyren)]^+$	H_2pyren	$[Au(pyren)]^+$
(N-H)	3545; 3534	---	3178	---
(C-H)	2843; 2832	3003; 2988; 2944; 2932	2941; 2871	---
(C=N)	1646; 1651	1568; 1562	1641	1577

Table 4. ^{1}H-NMR and ^{13}C-NMR assignments and chemical shifts for H_2pyren and $[Au(pyren)]^+$ in acetonitrile-d_3 relative to TMS.

^{1}H Assignment	Integration	H_2pyren δ (ppm)	Multiplicity, J (Hz)	$[Au(pyren)]^+$ δ (ppm)	Multiplicity, J (Hz)	Δδ (ppm)
H6	4	3.74	s	4.41	s	0.67
H2	2	6.10	t, ^{3}J (3.2)	6.48	dd, ^{3}J (4.2, 2.1)	0.38
H3	2	6.43	dd, ^{3}J (3.4), ^{4}J (1.2)	7.07	d, ^{3}J (4.3)	0.64
H1	2	6.86	m	7.45	d, ^{3}J (1.4)	0.59
H5	2	8.08	s	7.85	s	-0.23
^{13}C Assignment		H_2pyren δ (ppm)		$[Au(pyren)]^+$ δ (ppm)		Δδ (ppm)
C6		61.4		62.5		1.1
C2		109.3		112.8		3.5
C3		113.6		125.6		12.0
C1		121.8		139.9		18.1
C4		130.6		143.3		12.7
C5		152.6		161.2		8.6

s = singlet, d = doublet, dd = double doublet, t = triplet, m = multiplet. $\Delta\delta = \delta_{complex} - \delta_{ligand}$

Table 5. IC_{50} values (in μM) for Au(III) compounds in tumorigenic cell lines.

Compound	A549	PC3	HEC1B	Balb/3T3	Others
H_2pyren	---	---	54.6	---	---
$[Au(pyren)]^+$	39.0	35.8	28.0	37.2	---
$[Au(TPP)]^+$	---	---	---	---	0.13[a]
$[Au(bipy)Cl_2]^+$	125[b]	---	---	---	---
$[Au(en)Cl_2]^+$	125[b]	7.5[c]	---	---	---
$[Au(dach)Cl_2]^+$	125[b]	8.1[d]	---	---	---
$[Au(en)_2]^{3+}$	---	1.0[c]	---	---	---
Cisplatin	64[e]	0.18[f]	26[g]	---	27[h]

[a] Ref. 61; [b] Ref. 62; [c] Ref. 63; [d] Ref. 64; [e] Ref. 65; [f] Ref. 66; [g] Ref. 67; [h] Ref. 40.
TPP = tetraphenylporphyrin, bipy = 2,2´-bipyridine, en = ethylenediamine, dach = 1,2-diaminocyclohexane.